Magazine of Civil Engineering. 2019. 85(1). Pp. 61–71
Инженерно-строительный журнал. 2019. № 1(85). С. 61–71

Magazine of Civil Engineering

ISSN 2071-0305

journal homepage:http://engstroy.spbstu.ru/

DOI: 10.18720/MCE.86.6

Frost heaving of foundation pit for seasonal permafrost areas

G. Chao*, Z. Lu,
Shenyang Jianzhu University, Shenyang City, Liaoning, China
** E-mail: guochaoglovel@126.com*

Keywords: frost heaving; foundation pit; temperature field; temperature stress.

Abstract. Frost heaving can cause support structures to crack and even instability of the foundation pit. This paper describes the frost heaving features of the steel pile pre-stressed tendon composite foundation pit support system (SPPTCFPSS). As a combined rigid–flexible support system during the overwintering stage in Northeast China, these systems were used to investigate the transient heat conduction and fixed boundary one-dimensional frost heaving stress equations. The axial force sensors of the tendons used for the in-situ test accurately recorded the changing values of the axial forces of the pre-stressed tendons during the integrated working period for the foundation pit frost-heaving effect. Practical support data for the frost heaving stress analysis of the system were thus provided. The thermo-physical properties were obtained from the soil experiments, including the coefficient of thermal conductivity, specific heat of the foundation soil, and thermal expansion factor, among others. Base on this, the fluid effective velocity, saturation, and temperature fields were received from the heat flow coupling analysis of finite element methods (FEM).The results show that the actual axial force applied to the SPPTCFPSS is approximately equal to the theoretical value of the pit frost-heaving force calculated for the one-dimensional fixed boundary conditions corrected by saturation index from FEM. The SPPTCFPSS can adapt to a large-scale frost-heaving deformation to enable a reasonable increase in adaptive capacity in a region that has seasonal periods of frozen soil.

1. Introduction

Figure 1. Map of the project.

Chao, G., Lu, Z. Frost heaving of foundation pit for seasonal permafrost areas. Magazine of Civil Engineering. 2019. 86(2). Pp. 61–71. DOI: 10.18720/MCE.86.6.

Чао Г., Лу Ч. Морозное пучение котлованов в регионах сезонного промерзания грунтов // Инженерно-строительный журнал. 2019. № 2(86). С. 61–71. DOI: 10.18720/MCE.86.6

The utility tunnel project between Shenben Industry Greet in Benxi city, Liaoning province, China, and Liangjia Bridge is an important part of the Weining utility tunnel and is of great significance for the environmental protection and social development of the Benxi region. The utility tunnel constructed parallel to the Taizi river traverses a 6.2 km length of seasonal frozen soil region at 41°N (latitude) and an altitude higher than 150 m, as shown in Figure 1; a region of the Changbai mountains that experiences a relatively cold environment compared to the same latitude in a plain with five months of winter presents challenges associated with the mechanical sensitivity of geotechnical engineering measures to temperature variation. Under conditions of a seasonal frozen region at the high latitudes, engineering structures are forced to consider the threat of subsidence resulting from frost heaving and deformation of the underlying frozen soil foundation [1-4]. In response to such threats, lowering the deformation of the frozen foundation soils seems, in most cases, to present an effective approach for increasing the stability of the foundation pit in the seasonal frost region [5–8].

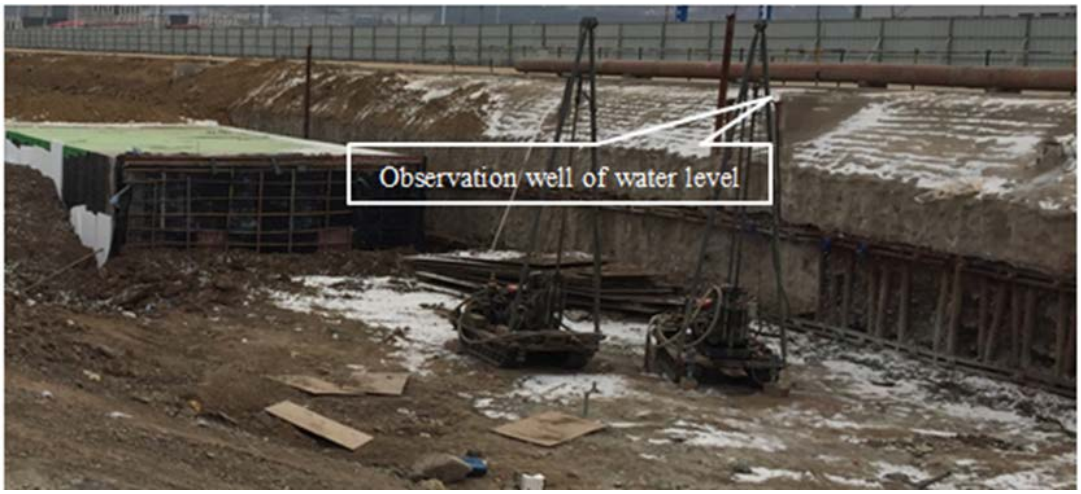

Figure 2. In-situ observation.

The foundation pit is located 50 m away from the south bank of the Taizi River; the depth of the pit is about 7 m, and the bottom elevation is 5 m below the water level. The soil layer formation shows that soil at a depth of 0–5 m is silt, 5–10 m is clay, and 10–12.5 m is gravel permeable layer. From this soil foundation information and observation well of water level, as shown in Figure 2, the capillary ascent zone (CAZ) or saturated frost zone (SFZ) is located between the capillary head and saturation lines, and the Taizi river provides the water resource for the freezing front of the foundation pit.

Many engineering measures have been proposed to protect foundation pits during the overwintering stages that underlie engineering infrastructures, and the effectiveness of some of these measures has been previously verified through field applications [9-13]. Among these, steel pipe piles with pre-stressed tendons that constitute a rigid-flexible composite supporting system, are considered one of the most efficient measures, as shown in Figure 3.

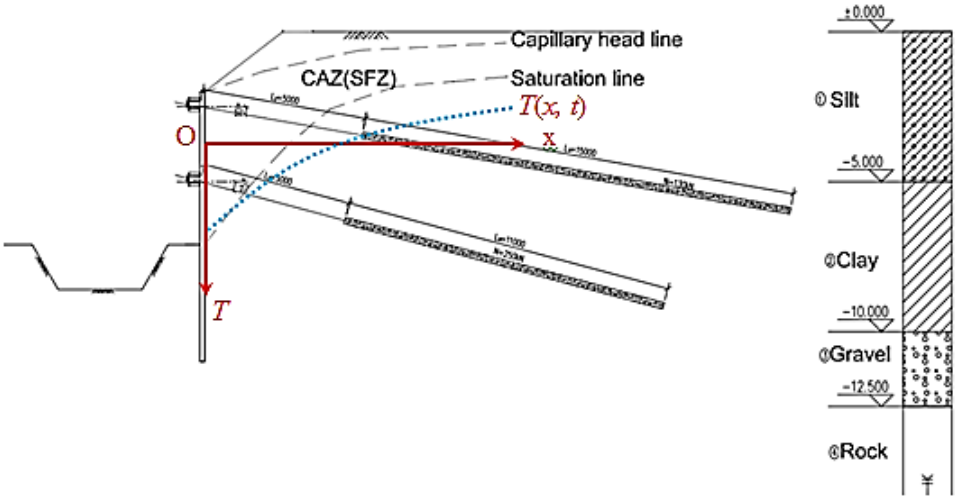

Figure 3. Profile of SPPTCFPSS.

Owing to the greater ability of steel to adapt to deformation than concrete, a steel pile pre-stressed tendon composite foundation pit support system (SPPTCFPSS) can adapt better to deflections from the frost heaving of the soils and synchronously maintain the stability of the foundation pit, while requiring no additional equipment and being easily realizable in construction projects. The existing protection measures

for overwintering foundation pits include straw bags, extruded Expanded Polystyrene heat-preservation boards, granulated foam-glass ceramics [14–15], and other passive heat insulation measures, or heating tropics, hot water pipes, and other active heat insulation measures. However, all these insulation measures increase project costs and carbon emissions. A rigid–flexible composite supporting system has the advantages of low carbon emission and environmental friendliness for adapting to frost heaving deformations of foundation pits in winter.

Once the winter season has passed, this composite support system can return to the initial displacement state automatically. However, this system requires foundation pit over-digging, so predictions of the deflection of the support system are required in advance.

2. Methods

The precondition of foundation pit frost heaving analysis is to determine the location of the CAZ and SFZ accurately, in order to determine the saturated and unsaturated areas in the foundation pit. In this analysis, the finite element method (FEM) with ABAQUS was first used to analyze and calculate the seepage field in the foundation pit. The results are shown in Figures 4 and 5. The physical parameters of the soil sample are summarized in Table 1.

Table 1. Physical parameters of soil sample.

w	n	s_w	w_l	w_p	c	$ø$	k
%	%	%	%	%	kPa	°	m/s
34.5	41.86	98	40	18	24.7	11	1×10^{-6}

In Table 1, w is the water content of soil, n is the porosity, s_w is the saturation, w_l is the liquid limit moisture content, w_p is the plastic limit moisture content, c is the cohesion, $ø$ is the internal friction angle, and k is the permeability coefficient.

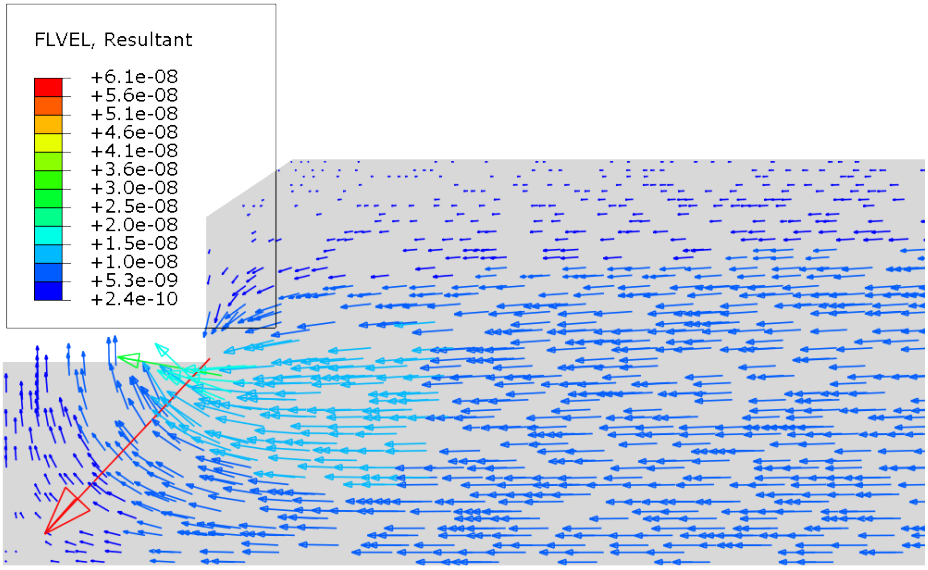

Figure 4. FLVEL of foundation pit.

In Figure 4, FLVEL denotes the current magnitude and components of the pore fluid effective velocity vector. The maximum value is 6.1×10^{-8} m/s, which occurs at the corner of the foundation pit. At the wall of the foundation pit, the direction of most velocity vectors is downward, while at the bottom of the foundation pit, the vectors' direction is upward. The comparison between Figures 4, 2, and 3 shows that the FEM results are consistent with the field foundation pit water level monitoring results. Because Taizi River is located 50 m outside the pit, the water level difference between the pit bottom and the river is 5 m, the hydraulic gradient is 0.1, and the permeability coefficient is small, the seepage water can be drained through the precipitation in the pit to ensure that the pit bottom is dry.

In Figure 5, SAT denotes the saturation of the foundation pit soil; the variation ranges from 1.0 to 0.33. The saturation curve is basically the line between the corner of the foundation pit and the river water level. The unsaturated curve is essentially parallel to the saturated curve, showing a linear decreasing trend, decreasing to the minimum value of 0.33 at the highest point, and the average value at the pit wall position is 0.68.

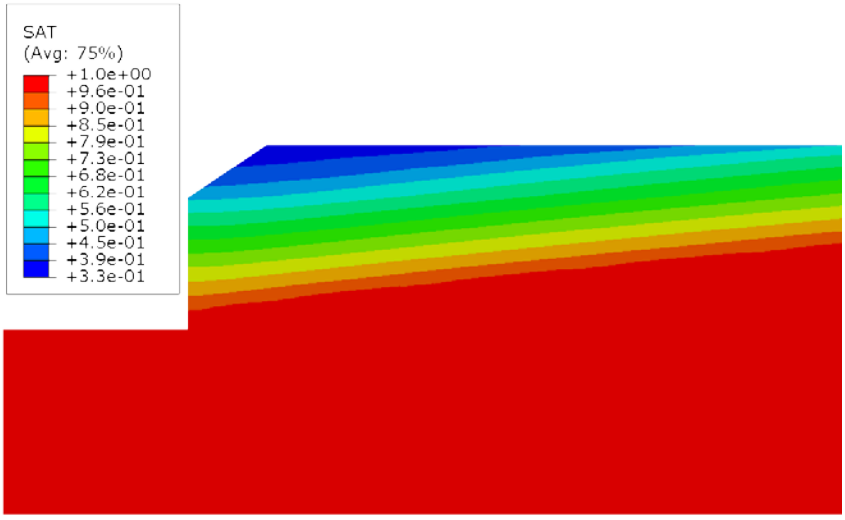

Figure 5. SAT of foundation pit.

The SPPTCFPSS is used in the natural environment during winter, so it is influenced by solar radiation and atmospheric temperature. Heat is generally transferred from the surface of the foundation to the depth, and converted with air. Therefore, it is necessary to analyze the temperature field of the system. The basic principle of the effect of temperature on a foundation pit is illustrated in Figure 3. The horizontal direction of the section shown is set as the x-axis and the vertical downward direction is the T-axis. The temperature field of the system was then obtained by the following equation [16, 17]:

$$\frac{\partial T}{\partial t} = a \cdot \left(\frac{\partial^2 T}{\partial x^2} \right), \tag{1}$$

where $T(x,t)$ is the temperature distribution function of the system,t is a temporal variable, and a is the temperature coefficient of the soil.

$$a = \frac{\lambda}{c_v}, \tag{2}$$

where λ is the heat conductivity coefficient and c_v is the volumetric heat capacity of the soil.

Substituting (2) into (1), we get

$$q_{\Sigma} = q_{sr}(t) - q_{ti}(t) + q_{hc}(t) = \lambda \frac{\partial T}{\partial x}, \tag{3}$$

where q_{Σ} is the sum of the heat flux of the foundation surface including solar radiation (SR) $q_{sr}(t)$, thermal irradiation $q_{ti}(t)$, and heat convection (HC) $q_{hc}(t)$, and λ is the coefficient of heat conductivity (CHC) in the present system, defined by

$$\lambda = \lambda_s - n\left[\lambda_s - s_w \lambda_i - \left(1 - s_w\right) \lambda_g \right], \tag{4}$$

where λ_s = 1.8 W/(m·K),λ_i= 2.2 W/(m·K), and λ_g= 0.02 W/(m·K) are the soil, water, and gas heat-conductivity coefficients, respectively, and λ = 1.92 W/(m·K) by equation (4) .

SR is considered the short-wave energy propagated to Earth from the Sun, and the amount of energy absorbed by the pit surface depends on its thermal properties and color

$$q_{sr}(t) = q_{sr0} \cos m\omega \left(t - 12\right) \quad 12 - \frac{c}{2} \le t \le 12 + \frac{c}{2}, \tag{5}$$

where q_{sr0} is the peak SR during daytime (q_{sr0}= 0.131 mQ), Q = 2.7×10^6(J/m^2) is the total SR during the day of winter, m = 12/c = 2 (c is the actual effective sunshine hours in a day, which is 6 h for winter), $\omega = 2\pi/24$ (rad) is the earth's self-rotation frequency, and q_{sr0} = 0.707×10^6(J/m^2).

$$q_{sr}(t) = q_{sr0} \cos \frac{\pi}{6}\left(t - 12\right) \quad 9 \le t \le 15\,. \tag{6}$$

The thermal irradiation q_{ti} of the present system consists of long-wave heat flux between the foundation pit surfaces and the sky. The total irradiation is thus considered in accordance with the Stefan–Boltzmann law as follows:

$$q_{ti} = \gamma\varsigma[(T_1|_{x=0})^4 - (T_a)^4], \tag{7}$$

where $T_1|_{x=0}$ is the foundation pit surface temperature, $\varsigma = 5.6697\times10^{-8}$ W/(m^2·K^4) is the Stefan–Boltzmann constant, and γ = 0.6 is the surface emissivity of the foundation pit surface.

The heat convection on the foundation pit surface is given by

$$q_{hc} = h_{hc}(T_a - T_s), \tag{8}$$

where $h_{hc}$is the convection coefficient, W/(m^2·K), T_a is the air temperature (AT), and it is measured in-situ with a thermometer as shown in Figure 4. T_s is the surface temperature of the foundation pit.

The AT measurement curves during the winter months of December, January, and Februaryin the project area are shown in Figure 6.

It can be seen from Figure 6 that, in December 2017, the highest AT is 277 K, lowest AT is 254 K, and daily variation is approximately 15 K. The highest temperature is 275 K in January 2018, lowest temperature is 246 K, and daily variation is approximately 12 K. February 2018 has a maximum temperature of 278 K, minimum temperature of 250 K, and daily variation of approximately 12 K.

At the beginning of December, the ground temperature dropped to 273 K, and the shallow groundwater began to freeze. The lowest temperature in winter occurs from late January to early February, the temperature starts to rise by mid-February, and rises to 273 K by the end of February.

Because foundation pit freezing is mainly caused by low temperature accumulation, the above daily temperature change curves need to be converted into an accumulated temperature curve, and the results are as shown in Figures 7–9.

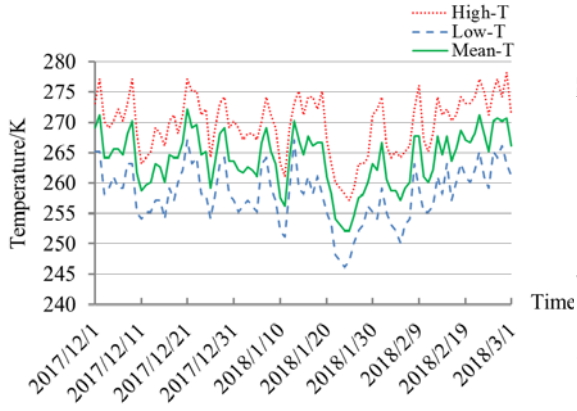

Figure 6. Air temperature.

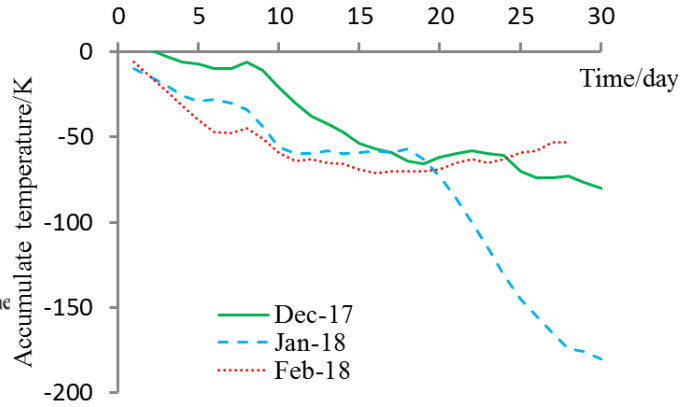

Figure 7. Daily highest temperature accumulation curves.

As seen in Figure 7, for December 2017 to January 2018, the daily highest temperature accumulation curves gradually fell; the temperature dropped dramatically in late January, with −50 K to −200 K change at this time for the wintering period, to the detriment of the foundation pit. By the middle of February, the temperatures began to rise, and the cumulative temperature curve rose gradually.

As seen in Figure 8, for December 2017 to January 2018, the daily lowest temperature accumulation curves gradually fell, with −400 K to −600 K change, and by the middle of February, the temperatures began to rise as the cumulative temperature curve rose gradually.

From Figure 9, the daily mean temperature accumulation curve trends are seen to be somewhere in between the maximum and minimum values, with −200 K to −380 K change. Therefore, the lowest temperature in January 2018 had the maximum influence on the foundation-pit temperature field; it was thus selected as the external temperature condition in this seasonal permafrost foundation temperature-field analysis.

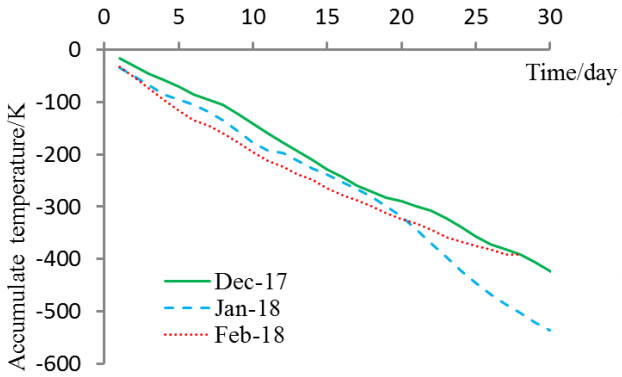

Figure 8. Daily lowest temperature accumulation curves.

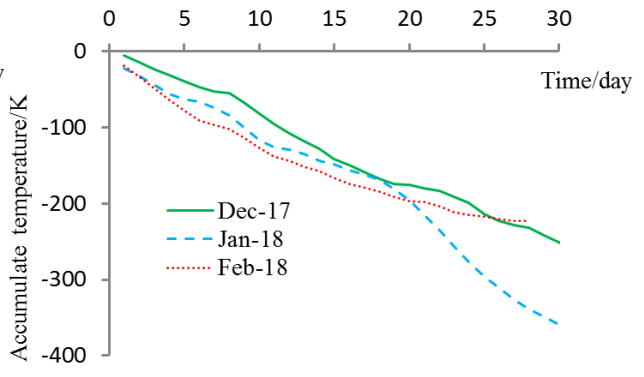

Figure 9. Daily mean temperature accumulation curves.

The parameter $h_{hc}$is a function of the local Reynolds number Re, thermal conductivity of air K_{air}, W/(m·K), Prandtl number Pr of air, and characteristic length of the medium on which the wind acts. According to the traditional heat-transfer theory, h_{hc} has two components, namely, free and forced convections. In this study, the Blasius solution was modified by combining the heat convection coefficients with the free and forced convections. The resultant heat-convection relationship can be expressed as

$$h_{hc} = 5.6 + 0.332\sqrt{\mathrm{Re}} \cdot \sqrt[3]{\mathrm{Pr}} \cdot \frac{K_{air}}{L}, \tag{9}$$

where K_{air}= 0.027 and Pr for air is 0.7. For airflow over an infinitely long flat plate, L = 0.15 m. The Reynolds number Re is given by

$$\mathrm{Re} = vL / \upsilon, \tag{10}$$

where v = 6 m/sis the local wind velocity, υ (m²/s) is the kinematic viscosity of air, which is usually 16.01×10⁻⁶, and Re = 56214, h_{hc} = 18 W/(m²·K).

Owing to the effect of SR, AT varies periodically. The lowest temperature during the day usually occurs at 4–6 a.m., whereas the highest temperature usually occurs approximately 2 h after peak SR. Hence, in a duration of less than 10 h, AT increases from its lowest to the highest value, but subsequently requires more than 14 h to return to the lowest value. A single sine function is used to simulate this daily AT variation:

$$T_a = \overline{T}_a \sin\omega\left(t - t_0\right), \tag{11}$$

where $\overline{T}_a$ is the daily temperature variation amplitude and t_0 is the time between the occurrences of the highest SR and highest AT plus 7 h. The time between the highest SR and highest AT can generally be set to 2 h, so that t_0 = 9 h.

Substituting equations (6), (7), and (8) into equation (3), we get

$$T = \frac{2\overline{T}_a}{r} e^{-x\beta} \sin\left(\omega t + x\beta - \theta\right), \tag{12}$$

where r, β, θ, ψ_1, ψ_2, and S_t are the calculated parameters.

$$r = \sqrt{\psi_1^2 + \psi_2^2}; \tag{13}$$

$$\beta = \sqrt{\omega / 2a}; \tag{14}$$

$$\theta = arctg\left(\frac{\psi_2}{\psi_1}\right); \tag{15}$$

$$\psi_1 = \left(1 + S_t\right)\cos\left(2\beta x\right) - \xi \cdot \sin\left(2\beta x\right); \tag{16}$$

$$\psi_2 = \xi \cdot \cos\left(2\beta x\right) + \left(1 + \xi\right)\sin\left(2\beta x\right); \tag{17}$$

$$\xi = \frac{\lambda}{h_{hc}}\sqrt{\frac{\omega}{2a}}; \tag{18}$$

$$S_t = \frac{\lambda}{h_{hc}}\sqrt{\frac{w}{2a}}. \tag{19}$$

When the temperature decreases, the pore water in the soil freezes and forms a freezing front; as water flow continues to be replenished, the freezing fronts shift, and even the pore water is blocked to form ice lenses in the soil. After water turns to ice, volume expansion occurs with gradual decrease in temperature. When the boundary conditions are constrained, temperature stress is generated. Thus far, there have been many methods to calculate the frost heaving stress [18–21]. The principle of a one-dimensional compressive stress is as follows: the one-dimensional frost heave force under saturated conduction is calculated as

$$\sigma = \alpha \cdot E \cdot \Delta T, \tag{20}$$

where α is the coefficient of thermal expansion (CTE) of the foundation soil, E is the elastic modulus of the frozen soil, and ΔT is the magnitude of temperature change of the soil.

For the unsaturated soil, frost heaving is relatively complex. This study uses the saturation $s_w$of the foundation pit soil to correct the above formula, and the results are as follows：

$$\sigma_{sw} = S_w \cdot \alpha \cdot E \cdot \Delta T. \tag{21}$$

The CTE in the present system is defined by

$$\alpha = \frac{1}{L_0} \cdot \frac{dL}{dT} = \frac{d\varepsilon}{dT}, \tag{22}$$

where L_0 is the orienting length of the soil specimen under some special temperature, $dL/dT = d\varepsilon$,and ε is the strain.

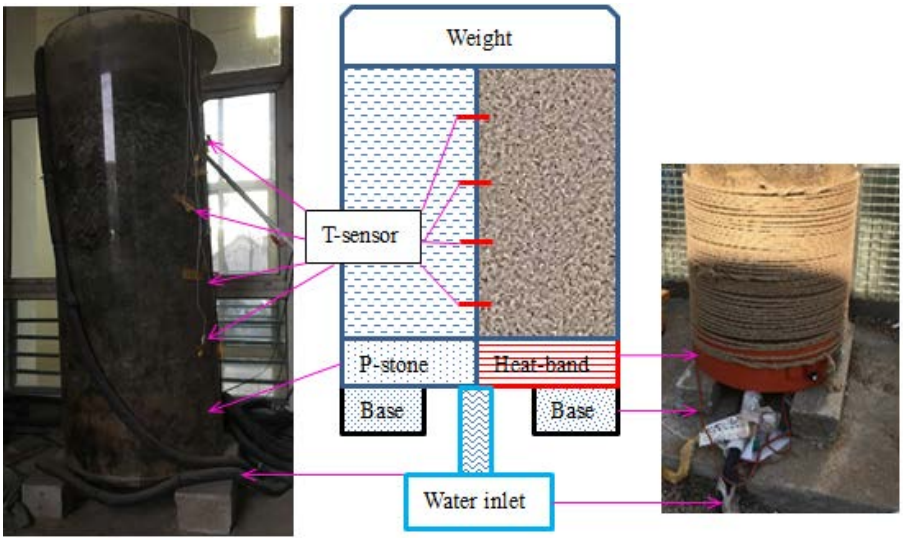

Figure 10. CTE and *E* test.

As shown in Figure 10, in this study, CTE and E were determined by an in-house test device. Refrigeration was used to ensure utilization of the natural winter environment in the project area, and the soil samples for the test were placed in an acrylic bucket with a diameter of 0.8 m, height of 2 m, and wall thickness of 1 cm. An inlet pipe, with electric and tropical packages to ensure the liquid state of the water, was arranged at the bottom of the bucket. A permeable stone was arranged between the water inlet pipe and the soil sample. The outer cylinder of the permeable stone enclosed an electric heating belt to prevent water from freezing at the site. The upper part of the permeable stone was filled with soil samples, and temperature sensors were embedded in the soil samples. A weight was set on top of the soil sample, and a deformation meter was set on top of the weight to observe the frost heave deformation.

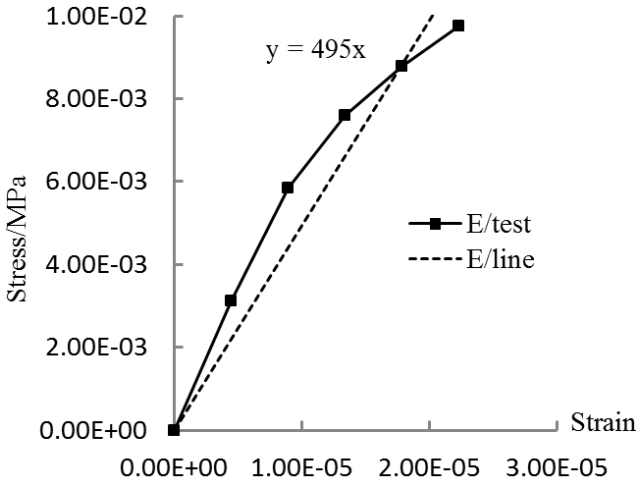

Figure 11. Elastic modulus E of frozen soil.

First, the surface elevation (*dL*) of the soil sample under the natural environmental condition in winter was observed; when dL stabilizes, it stops supplying liquid water, and CTE is calculated by formula (21). The temperature changes (dT) were measured with thermal sensors simultaneously. Then, the vertical deformation of the soil sample under the gravity of the weight was measured by stacking weights on the soil surface in order to calculate the value of E. The results are shown in Figure 11, the elastic modulus E = 495 MPa of frozen soil, measured with the in-house test device shown in Figure 10.

Assuming that all the frost heaving force is borne by the pre-stressed tendon, the axial force of the tendon is calculated as follows:

$$F = \int_0^D \sigma_{sw} \cdot S dx \,, \tag{23}$$

where S is the area of temperature stress assumed by each tendon and D is the depth of the freezing front of the foundation.

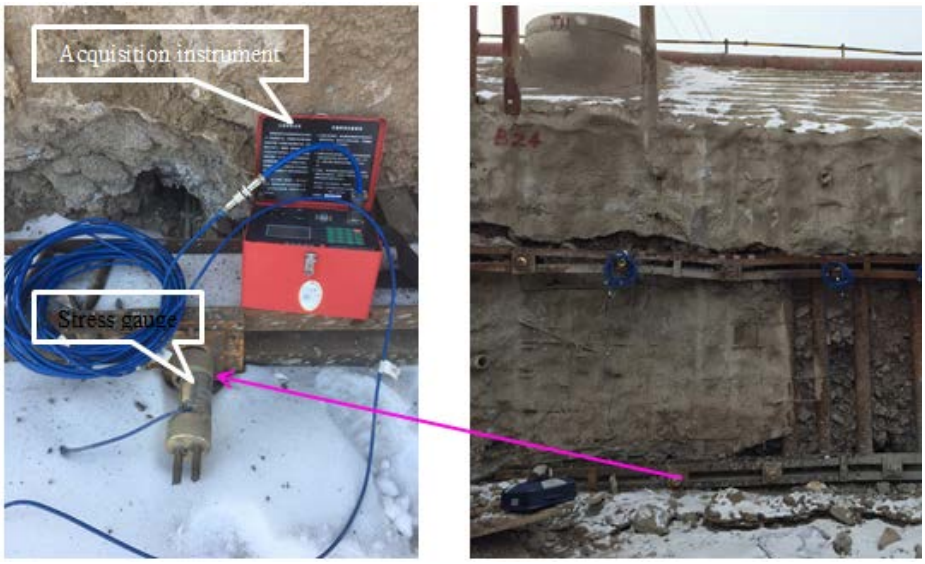

Figure 12. Tendon axle force test.

As shown in Figure 12, the axial force variations of pre-stressed tendons for the temperature stresses of foundation soils were measured using vibrating wire tendon stress gauges (JMZX3102HAT) with a range of 200 kN, sensitivity of 0.1 kN, and accuracy of 0.4 kN. Internally installed semiconductor temperature sensors were used for automatic temperature correction, and the data acquisition instrument (JMZX-3006) produced by Kingmach Measurement & Monitoring Technology Co., Ltd, was used to gather data.

The pre-stressed tendons are two stranded wires, each with a diameter of 15.2 mm and tensile strength of 1860 MPa, with a transverse spacing of 1.2 m and vertical spacing of 2 m. Each pre-stressed tendon resists a foundation pit compressive stress of 2.4 m^2.

The monitoring period of axial force of the pre-stressed tendon was from October 21, 2017 to March 14, 2018, when the initial tension of the anchor cable began. The monitoring frequency was once a week.

3. Results and Discussion

The thermo-physical parameters are summarized in Table 2.

Table 2. Thermo-physical parameters.

λ	c_v	E	ρ	h_{hc}	α
W/(m·K)	J/(kg·m^3)	MPa	kg/m^3	W/(m·K)	1/ K
1.92	1364	495	1.7×10^3	21	21×10^{-6}

The temperature field results of SPPTCFPSS are analyzed using equation (12) and FEM on ABAQUS for relative material variables and boundaries, and the results are shown in Figures 13 and 14.

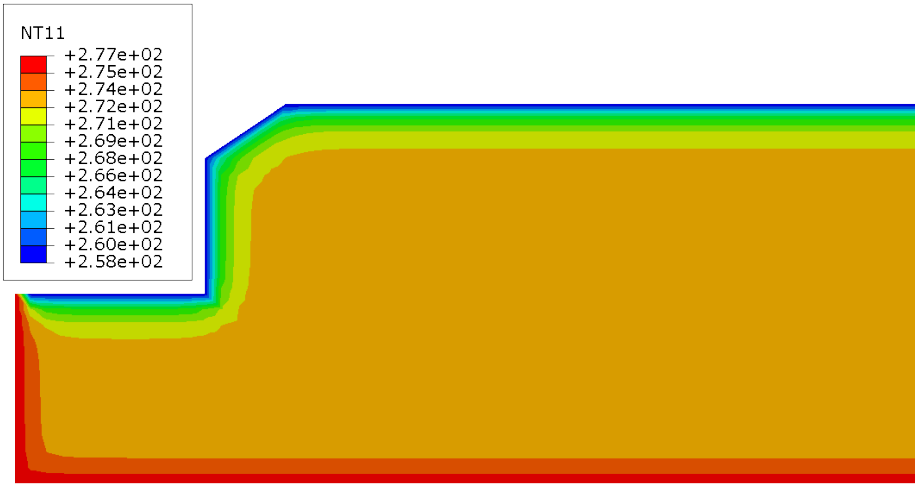

Figure 13. Temperature field in January 2018.

As can be seen from Figure 13, in January 2018, the temperature field of the foundation pit system gradually decreases from 258 K to 277 K along the outer boundary of the foundation to the distance. The boundary temperature is the same as the AT of 258 K, and the severe impact temperature area is within the range of 2 m near the foundation pit boundary, where the temperature quickly dropped to the freezing point of 273 K.

As can be seen from Figure 14, the temperature of the foundation pit system gradually decreases with the increase in depth, and the freezing depth ranges from 1.4 m to 2 m. The above freezing depth level is nonlinear; the freezing depth temperature is also nonlinear. December and January temperatures (accumulated) decrease, the minimum being 258 K, and recovery happens in February, with the lowest temperature being 269 K. As AT drops to zero in November, ground surface temperature from the surface to freezing front gradually decreases; the surface temperature in December fell to 263 K, the frozen depth was 1.8 m, and after that the earth's surface temperature fell down to 258 K in January, and the frozen depth was 2.0 m, simultaneously. At the beginning of February, with the increase in AT, the ground surface temperature increases too, but due to the heat capacity of the foundation, the curve of temperature distribution along the direction of depth exhibits a reverse bending change, showing a trend that the temperature change in the foundation lags behind the temperature change. The changing characteristics of the above temperature space-time curve scientifically reflect the influence of the temperature accumulation effect on the ground temperature field. The ground temperature below the freezing front gradually recovered from zero to 277 K and remained constant.

Temperature stresses according to the theoretically calculated value by equation (21) are shown in Figure 15. They gradually decrease to zero as the freezing front place is reached. The temperature stresses and temperature-field change rule are synergistic from December 2017 to January 2018, and increase gradually, then gradually decrease in February 2018; the maximum value occurs in January with 98 kPa. The above temperature stresses, on the conditions of the foundation pit with semi-infinite fully controlled one-dimensional boundary space, are the premise of the theoretical calculation results. However, as the scheme used here is to allow proper deformation of the support system, the actual temperature fields do not produce so much of the temperature stresses, and the axial force of pre-stressed tendons in the in-situ test and the ideal value from equation (23) are all shown in Figure 16.

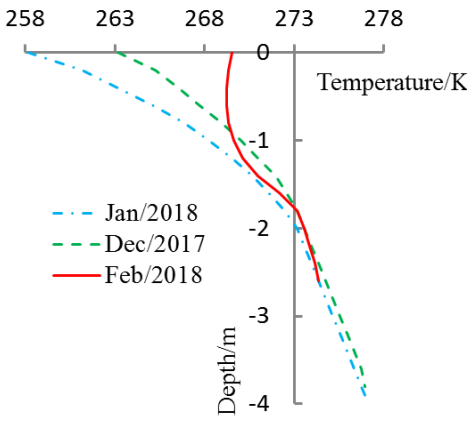

Figure 14. Temperature field.

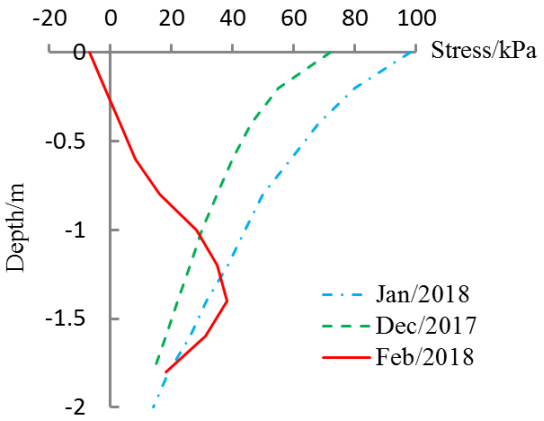

Figure 15. Temperature stresses.

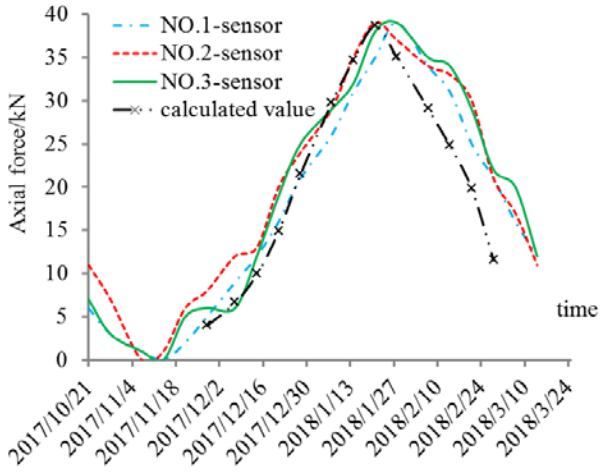

Figure 16. Axial force of pre-stressed tendons in-situ.

The axial force test results show that the three pre-stressed tendons are locked on October 21, 2017. Because of the relaxation of steel strands and anchorage segment of soil consolidation effect, the axial force of pre-stressed tendons fell by 8 kN in mid-November. The frost heaving of the foundation makes the axial force increase gradually in late January 2018 to a peak of 38 kN, with recovery in the middle of March 2018 to 12 kN, as shown in Figure 13. However, according to equation (23), which is used to calculate the frost heaving force value, each pre-stressed tendon gives an axial force of 39 kN, and the actual measured value is 38 kN. Thus, an agreement with theoretical calculation is seen. The temperature stress of the foundation pit soil based on one-dimensional fixed boundary calculation is corrected by the saturation index of soil. Because the foundation soil above the infiltration line is in an unsaturated state after foundation pit dewatering, the effect of saturation on frost heave force should be taken into account when calculating soil frost heave.

4. Conclusions

1. The seepage field including CAZ and SFZ, which is the precondition of foundation pit frost heaving analysis, was analyzed accurately by FEM. Based on the transient heat conduction equation and indoor and outdoor thermo-physical tests, the temperature field of the foundation pit in a seasonal frozen soil area can be accurately calculated. The theoretical calculation of temperature stress based on one-dimensional fixed boundary conditions corrected by saturation index is accurate.

2. The rigid and flexible composite support system composed of pre-stressed tendons and steel pipe piles can effectively resist part of the temperature stress. The deformation of the foundation pit can be partially recovered under the action of pre-stressed tendons when the temperature rises, so this kind of supporting structure is suitable for the foundation pit in a seasonal frozen area.

3. The engineering in-situ monitoring temperature stress data applied to the SPPTCFPSS is approximately equal to the theoretical value of the pit temperature stress, which is calculated based on the one-dimensional fixed boundary conditions and corrected by the saturation index of the unsaturated zone in the foundation pit. Therefore, the calculated value based on the one-dimensional fixed boundary temperature stress can be taken as the design value for the foundation pit support system.

References

1. Ivanov, K.S. Granulated foam-glass ceramics for ground protection against freezing. Magazine of Civil Engineering. 2018. 79(3). Pp. 95–102. DOI: 10.18720/MCE.79.10
2. Zhussupbekov, A., Shakhmov, Z., Tleulenova, G. Geotechnical problems on freezing ground soil and experimental investigation in Kazakhstan. Sciences in Cold and Arid Regions. 2017. No. 3(9). Pp. 331–334.
3. Guo, L., Zhang, Z., Wang, X., Yu, Q., You, Y, Yuan, C., Xie, Y., Gou, T. Stability analysis of transmission tower foundations in permafrost equipped with thermosiphons and vegetation cover on the Qinghai-Tibet Plateau. International Journal of Heat and Mass Transfer. 2018. No. 121. Pp. 367–376.
4. Yu, Q., Ji, Y., Zhang, Z., Wen, Z., Feng, C. Design and research of high voltage transmission lines on the Qinghai–Tibet Plateau–A Special Issue on the Permafrost Power Lines. Cold Regions Science and Technology. 2016. No. 121. Pp. 179–186.
5. Rui, D., Deng, H., Nakamura, D., Yamashita, S., Suzuki, T., Zhao, H. Full-scale model test on prevention of frost heave of L-type retaining wall. Cold Regions Science and Technology. 2016. No. 132. Pp. 89–104.
6. Tretyakova, O.V., Yushkov, B.S. Inverted-cone piles for transport constructions in seasonally freezing soils. Soil Mechanics and Foundation Engineering.2017. No. 3. Pp. 18–21.
7. Zhenya, Liu, Jiankun, Liu, Xu, Li. Experimental study on the volume and strength change of an unsaturated silty clay upon freezing. Cold Regions Science and Technology. 2019.No. 157. Pp. 1–12.
8. Zhang, S., Sheng, D., Zhao, G. Analysis of frost heave mechanisms in a high-speed railway embankment. Canadian Geotechnical Journal. 2016. No. 53. Pp. 520–529.
9. Batenipour, H., Alfaro, M., Kurz, D. Deformations and ground temperatures at a road embankment in northern Canada. Canadian Geotechnical Journal. 2014. No. 51. Pp. 260–271.
10. Zheng, H., Kanie, S., Niu, F. The thermal regime evaluation of high-speed railway foundation by mixed hybrid FEM. Cold Regions Science and Technology. 2018. No. 155.Pp. 333–342.
11. Nishimura, S., Gens, A., Olivella, S. THM-coupled finite element analysis of frozen soil: formulation and application. Ge´otechnique. 2009. 59(3). Pp. 159–171.
12. Lackner, R., Amon, A., Lagger, H. Artificial ground freezing of fully saturated soil: thermal problem. Journal of Engineering Mechanics. 2005. 131(2). Pp. 211–220.
13. Kong, Q., Wang, R., Song, G. Monitoring the soil freeze-thaw process using piezoceramic-based smart aggregate. Journal of Cold Regions Engineering. 2014. 28(2). Pp. 1–16.
14. Crandell, J.H. Below-ground performance of rigid polystyrene foam insulation: review of effective thermal resistivity values used in ASCE standard 32-01–design and construction of frost-protected shallow foundations. Journal of Cold Regions Engineering. 2010. 24(2). Pp. 35–53.
15. Liu, Z., Yu, X., Sun, Y. Formulation and characterization of freezing saturated soils. Journal of Cold Regions Engineering. 2013. 27(2). Pp. 94–107.
16. Zhang, M., Guo, C., Yu, B., etc. CTCP temperature fields and stresses. International Journal of Pavement Research and Technology. 2017. No. 3(3). Pp.553–562.
17. Chen, J.-Q., Li, L., Zhao, L.-H., Dan, H.-C., Yao, H. Solution of pavement temperature field in “Environment-Surface” system through Green’s function. Journal of Central South University. 2014. 21(5). Pp. 2108–2116.
18. Tretiakova, O.V. Normal stresses of frost heaving as function of excess moisture. Magazine of Civil Engineering. 2017. 76(8). Pp. 130–139. DOI: 10.18720/MCE.76.12
19. Ghoreishian Amiri, S.A., Grimstad, G., Kadivar, M. Constitutive model for rate-independent behavior of saturated frozen soils. Canadian Geotechnical Journal. 2016. No. 53. Pp. 95–102.
20. Scott Crowther, G. Lateral pile analysis frozen soil strength criteria. Journal of Cold Regions Engineering. 2015. 29(2). Pp. 11–23.
21. Shelman, A., Tantalla, J., Sritharan, S. Characterization of seasonally frozen soils for seismic design of foundations. Journal of Geotechnical and Geoenvironmental Engineering. 2014. No. 140(7). Pp. 1–11.

Contacts:

Guo Chao, 86-24-24692693; guochaoglovel@126.com
Zhengran Lu, 86-24-24692693; luzhengranglovel@126.com